Sampling vacancy configurations with large relaxations using Smart Darting

Döme Tanguy

Sampling vacancy configurations with large relaxations using Smart Darting

D. Tanguy[1, *]

[1] *Univ Lyon, Université Claude Bernard Lyon 1, CNRS, Institut Lumière Matière, F-69622, VILLEURBANNE, France*

(Dated: October 1, 2023)

Markov chain Monte Carlo simulations, combining the sampling of the position of the particles and their chemical nature, are very useful when calculating, for example, average site occupancies at crystalline defects in alloys. Unfortunately, when the relaxations around the solutes are large, the exchange moves can be systematically rejected because of atoms overlapping. As a consequence, the simulations are often trapped in nonphysical configurations. In this paper, the "Smart Darting" method from Andricioaei et al. is adapted and extended to propose a solution to this limitation. The method is tested in a particularly demanding case: the sampling of the arrangements of delocalized vacancies and divacancies in grain boundaries, both in the fcc and the bcc structure. Beyond the methodological aspects, intergranular vacancy clusters are interesting in several contexts such as ductile fracture, irradiation or thin film dewetting, and therefore several properties have been measured that can be useful for mesoscale modeling: segregation energies, effective diffusion barriers in and out of the grain boundaries, vacancy-vacancy binding energies and elastic dipole tensors.

I. INTRODUCTION

Vacancy clusters and voids, particularly at interfaces, are important in various contexts. They are at the origin of crack embryos in plasticity related fractures: they form at dislocation boundaries during ductile fracture of pure metals [1, 2] and at the interface between the matrix and persistent slip bands in the early stages of fatigue crack formation [3]. In the presence of interstitial solutes, they can also lead to the formation of bubbles. Miura et al. [4] have shown by microtensile testing of individual grain boundaries that a critical He bubble size and intercavity spacing, in the 5 nm range, can induce a transition from ductile fracture to intergranular brittle fracture, with a drop in fracture toughness. The phenomenon can be reproduced, to some extent, by atomistic simulations with voids only [5]. In the case of hydrogen embrittlement, the role of nanoscale bubbles is less obvious [6] but it was shown that submicron dislocation cells are formed along the brittle crack path [7, 8] and nanoscale roughness was measured on the fracture surface [9]. Therefore, understanding how vacancies cluster along interfaces (cell walls and grain boundaries) under the influence of stress and temperature is important for modeling fracture in many different conditions.

Atomistic simulations are tools of choice, with their limitations, for addressing this question. Much has been learned about single vacancies in interfaces. In fcc metals, they diffuse preferentially along dislocation cores but also along the stacking fault ribbons. The activation energy is slightly reduced in comparison to the bulk [10–12] but the mechanism remains a simple vacancy-first neighbor exchange, i.e. the relaxations of the neighbors are marginal [11]. The situation is quite different in grain boundaries [13]. The relaxations are often large, especially in the configurations of low energy (the most statistically visited), and to such an extent that the vacancies are said to be "delocalized" [14, 15]. Furthermore, some grain boundary sites cannot host stable vacancies. This can lead to long diffusion jumps where several atoms are displaced [13, 16]. At increasing temperature, the crystalline order within the core of the GBs is much lower than that in the bulk and continuously decreases until melting [13]. Stringlike cooperative motions of atoms, which are different from the long jumps at low temperature, are activated [17, 18]. It was also shown that a grain boundary emerging at a free surface, which acts as a source of point defects (interstitials in this case), can transition with temperature between different structures. The reverse transformation could be obtained by absorbing vacancies [19]. More generally, it is well known that the construction of a grain boundary, defined by a set of macroscopic geometric parameters, requires the optimization of the energy with respect to microscopic parameters which are the relative translation of the two grains, plus the number of atoms within the interface [20]. Recently, not only the lowest energy structures but also all metastable structures [21, 22] were found. The structural unit model was generalized and its ability to predict the stable and metastable structures of families of tilt boundaries, as a function of the misorientation angle, was established. The large number of these metastable structural units and the quasi-continuous spectra of their excess energies, indicate that mixtures of such structures should exist at non zero temperature. Since they can also have different numbers of atoms, the mixing of structural units could be an efficient way of accommodating vacancies. This is of particular interest for designing materials resistant to irradiation [23–26]. In this context, detailed studies of the absorption of vacancies were conducted in a fcc-bcc interface composed of a network of misfit dislocations. Delocalized vacancies were not found to attract each other, although misfit dislocation intersections constituted preferential segregation sites [25]. In addition,

* dome.tanguy@univ-lyon1.fr

mixed tilt/twist GBs in Cu [26] were submitted to the absorption of large quantities of vacancies. The same GB core structures were visited periodically during vacancy loading when the GB changed structure by translation and shear. Both studies show that grain boundaries can be tolerant to large quantities of vacancies. Note that no void formation was found by Molecular Dynamics. In the bulk, experimentally, void formation appears when a critical vacancy concentration, in the range of 10^{-2}, and at a high enough temperature, is reached [27]. Simple atomic kinetic Monte Carlo and simulations of phase demixion by atomistically informed Cahn-Hillard equations can qualitatively reproduce the phenomenon [28].

Most of the valuable results summarized above have been obtained by Molecular Dynamics (MD). However, this method has well known limitations, particularly concerning the limited timescale, which is somewhat compensated by working at high temperature. In this case, the grain boundaries are populated by defects, in addition to the vacancies deliberately introduced in the system. They complexify the analysis and influence the mechanisms that constitute unwanted side effects if the interest is in the low temperature behavior. Few studies of interfacial vacancies use elaborate, but outdated, versions of MD [12, 16], such as hyper-MD or temperature-accelerated dynamics. These methods have evolved [29, 30] and, combined with Adaptative Kinetic Monte Carlo (AKMC) [31, 32], have successfully simulated the dynamics of vacancies in a thin slab, in particular the re-entry of vacancies from the surface into the subsurface on the microsecond timescale [33]. Nevertheless, they might still be limited by the "low barrier" problem in the case of grain boundaries because of the transitions between SUs or by the massive number of transition searches necessary for AKMC. When only clustering tendencies are searched and not a realistic dynamics, Markov chain Monte Carlo, where the full phase space is sampled (i.e., site occupancies and relaxations), is very useful [34]. For example, in the semigrand canonical ensemble, it was used to study intergranular segregation [35, 36]. Nevertheless, it suffers from the limitation of the vanishing acceptance rate of exchanges when relaxations around solutes are large, which is the case for delocalized vacancies.

In this context, we present a simulation methodology that overcomes the trapping issue of Markov chain Monte Carlo (MCMC). In the first part of the paper, the method is detailed and illustrated in the case of a vacancy occupying a peculiar GB site where it can be in two states: one localized and another delocalized. The power of the method is demonstrated as it succeeds in sampling, with a high acceptance rate, the occupancy of different crystallographically equivalent positions, in the delocalized state. Then, the average vacancy occupancies corresponding to the equilibrium between the GB site and a bulk site are calculated by exchange moves using two different paths: one going through the localized state and another going through the delocalized state. The energy barrier between the localized/delocalized vacancy states can be tuned by changing the strain perpendicular to the interface in such a way that the two states can be equilibrated by atomic displacement moves only. In this condition, the occupancies calculated by the two different paths should be equal. This demonstrates that the method and its implementation are correct. In the second part of the paper, the method is used to study single and divacancies in 4 grain boundaries in Al (fcc) and in bcc Fe. The efficiency is measured and the clustering tendency, which is quite different from one GB to another, is analyzed.

II. MONTE CARLO METHOD

The method combines three aspects: the classical Monte Carlo simulation of the (N,V,T) ensemble by sampling the particles' positions [34], a periodic search for local energy minima, and finally transitions between these energy minima by the Smart Darting method [37] (Fig.1). In the following each of these aspects is detailed.

The starting point is the classical Monte Carlo simulation of the (N,V,T) ensemble [34, 38]. The definition of the microstates was modified to introduce vacancies [39]: the volume V is split into Voronoi cells according to the stable crystalline structure. The N vectorial positions of the particles are replaced by N displacements with respect to the lattice nodes. It is implicitly considered that a Voronoi cell does not contain more than one particle. If this is not the case, the lattice should be refined by considering interstitial sites for example. The empty Voronoi cells are defined as vacancies. The set of N displacements is completed by a vector of M occupancies p_i such that $p_i = 1$ if the site is occupied, zero otherwise, and M is the number of sites contained in volume V. If the system contains a grain boundary (GB), the lattice is the one of the minimum energy GB structure [40]. The configuration space is composed of the permutations of the vacancies (a swap of the occupancies) and the volume of occupied Voronoi cells. The partition function to be sampled is:

$$\mathcal{Q}_M(N,V,T) = \sum_{\{p_n\}^M} \frac{1}{\Lambda^{3N}} \int_{vor} d\vec{u}^N \times exp(-\beta(\mathcal{H}(\{p_n\},(\vec{u})^N))) \quad (1)$$

where *vor* is the volume of the Voronoi cell surrounding each lattice site and Λ is the thermal de Broglie wavelength ($\Lambda = \sqrt{h^2/(2\pi m k_B T)}$), m is the mass of the particle, h and k_B are the Planck and Boltzmann constants. The sampling is done by proposing random displacement increments to a randomly selected particle within the Voronoi cell of the site (Δu moves) or swapping of occupancies between first neighbors (X moves). The energy variation is calculated and the moves are accepted according to the Metropolis criterion. Most of the time, a particle remains confined to the vicinity of the lattice node. If a particle attempts to cross a facet of

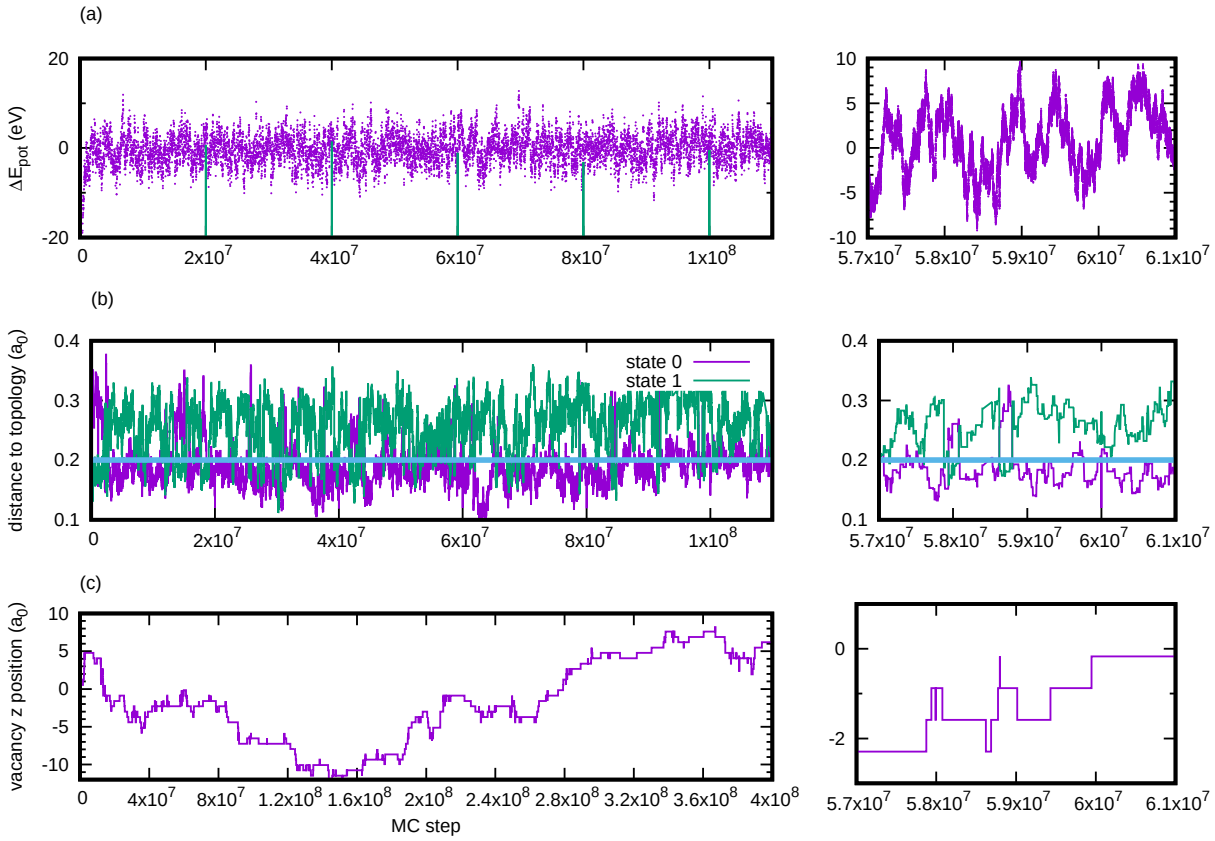

Figure 1. (Color online) Sampling of the configuration space of a system composed of the $\Sigma 33(5\bar{5}4)[110]$ symmetrical tilt grain boundary, under 3% strain with one vacancy. (a) Evolution of the energy (eV) as a function of the Monte Carlo steps, essentially because of Δu moves. Periodic energy minimizations are represented by vertical lines. (b) Evolution of the distance between the current microstate and states 0 (vacancy delocalized and on the most favorable GB site) and 1 (localized). The states are shown in figure 2. The Smart Darting parameter ϵ is set to 0.2 a_0. As a consequence, the system is usually within the neighborhood of state 0 or 1, and therefore, the number of Smart Darting moves attempts is close to the maximum. (c) Evolution of the z position of the vacancy, illustrating acceptance of Smart Darting moves between the vacancy and one of its first neighbors along the tilt axis. The comparison of the zooms (right pictures b and c) shows that Smart Darting moves are accepted whether they are performed between states 0 or between state 0 and 1 at different z positions.

the Voronoi cell toward a vacant site by Δu moves, the microstate is updated by swapping the site occupancies and modifying the displacements accordingly (vacancy displacements are zero). If the relaxations around the vacancies are small, this simple scheme is efficient [39]. Otherwise, the X moves are always rejected because of overlaps between particles, as shown below.

Smart Darting [37] is an efficient way of avoiding trapping along the Markov chain. Consider a list $\{X_0^i\}$ of local minima of the potential energy and neighborhoods of arbitrary size ϵ around them. A Smart Darting move (SD move) consists in checking with probability p_{SD} if the current microstate of the Markov chain is within ϵ of one of the minima. If not, the SD move is rejected (the current microstate is counted again in the Markov chain). If yes, for example X_0^i, another local minimum of the list is selected at random, for example X_0^j. The move performs a translation of the system from the neighborhood of size ϵ of X_0^i to the neighborhood of size ϵ of X_0^j. This is done by adding the "dart" $D = X_0^j - X_0^i$ to the current microstate, i.e. $X_{new} = X_{old} + D$. The corresponding energy variation is computed and the move is accepted/rejected according to the Metropolis rule. In our case, the "dart" is a combination of an occupancy swap (an exchange between a vacancy and a first neighbor for example) and a translation (the relaxations around the old position of the vacancy are canceled and the new relaxations are applied around the new position of the vacancy). In more detail, the structure of the GBs is periodic, particularly along the tilt axis for tilt GBs. The lattice sites are given an index that repeats periodically. The relaxations around the vacancies are collected, in the different configurations, after the energy has been minimized by a procedure that is detailed later. For a single vacancy, the configuration is defined by the index of the vacant site and the relaxations $\{\vec{u_0}\}$ of the neighbors. These are referenced by the index of the neighbor site and the z position of its lattice node, relative to the z of

the vacant site, called Δz. The ensemble given by the index of the vacancy and the list of (index,Δz, $\vec{u_0}$) of the neighbors is called a "topology", in reference to the kinetic-Activation Relaxation Technique [32]. The domain over which $\{\vec{u_0}\}$ is collected should be sufficiently large to contain all the sites that are significantly relaxed. Otherwise, the attempts will be systematically rejected because of overlaps of particles. For moving a vacancy from site i, first the distance to the different known topologies is evaluated as:

$$dist_k = \max_{(index,\Delta z)} \{\|\vec{u_0}^k - \vec{u}\|\} \quad (2)$$

where the distance is evaluated only for the topologies compatible with the distribution of the site occupancies, and k is the index in the list of topologies. If there exists a topology k_i where $dist_{k_i} < \epsilon$, then a site j, neighbor of i, is selected and a new topology is selected in the list of topologies (compatible with site j being occupied by a vacancy), referenced by k_j. The "dart" is then the combination of the swap of the occupancies of the lattice sites j and i and the translation (index, Δz, $\vec{u_0}^{k_j} - \vec{u_0}^{k_i}$). An example is given in Fig. 1b. In the specific GB studied, the vacancy can be in two states on the most favorable GB site, one "localized" with limited relaxations of the neighbors and one "delocalized". They are labeled states 1 and 0. So, for the same GB site index, there exists two topologies, shown in Fig. 2. The GB being a tilt GB of axis [110] of the fcc structure, such sites constitute a whole line of first neighbors. Figure 1b shows the fluctuation of $dist_0$ and $dist_1$ due to the Δu moves. The neighborhood size ϵ has been adjusted such that the system is usually either in state 0 or in state 1 so that SD moves can be attempted. This is done in the following way: starting from a microstate where the system is in the neighborhood of topology 0, for example, a first neighbor site is chosen at random, either above or below the actual vacant site and a new topology is selected at random for this site, for example topology 1. The "dart" is applied, i.e. the neighbors of the old vacant site are displaced by $-\vec{u_0}^0$ and the ones of the new site are displaced by $+\vec{u_0}^1$. The occupancies are switched between the two GB sites. The variation in the energy is calculated and the transition is accepted/rejected based on the Metropolis criterion. Figure 1c shows the one dimensional random walk of the vacancy obtained. The simulation also contains topologies that would let the vacancy escape from the grain boundary but this does not occur at that temperature (300 K).

An SD move can only be performed in between two already known topologies. Starting with no known topology, the Markov chain is constructed with Δu and X moves alone and is quickly trapped in a configuration where the vacancy is delocalized. The energy is minimized at regular intervals. Then, the topology around each vacancy is extracted and stored in the format given above. When several vacancies are present, a topology also contains a list of (index, Δz) for the other vacancies

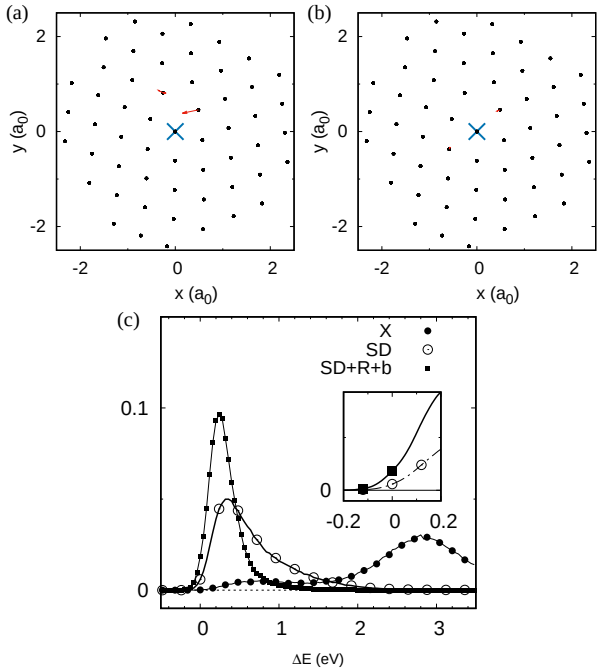

Figure 2. (Color online) Relaxations around a single vacancy (large cross) on the most favorable site of the $\Sigma 33(5\bar{5}4)[110]$ symmetrical tilt grain boundary, strained by 3% perpendicular to its plane. (a) State 0 ("delocalized vacancy") and (b) state 1 ("localized vacancy"). Displacement values larger than 0.05 a_0 are represented by arrows. They constitute, together with the site index, the topology used for the Smart Darting moves. (c) Distribution of the energy variation ΔE (eV) when a simple exchange (X), a simple Smart Darting exchange (SD) or a Smart Darting exchange plus the sampling of the neighbors, including the bias in the acceptance rule $-kT \log \frac{\prod(n\to o)}{\prod(o\to n)}$ (SD+R+b) (Eq. 7), are made. Only neighbors with a relaxation larger than 0.1 a_0 were considered and the acceptance rate was on the order of 5% at T=300K.

within the cutoff radius of the topology. If the topology is unknown, it is stored in the list of known topologies. Since it is the first time it is visited, there are few chances that other topologies appropriate for the SD move, i.e., with a vacancy in first neighbor position of the actual vacancy, exist in the list. Therefore, no SD move can be constructed from the information concerning the current configuration alone. In addition to the extraction of the current topology from the minimized configuration, a series of robust Nudged Elastic Band (NEB) calculations [41] between the current configuration and the ones obtained by swapping the vacancy with one of its neighbors (within the same range as the one for the SD move, which is not necessarily limited to first neighbors) is performed. If the NEB finds an intermediate configuration, the corresponding topology is extracted. Otherwise, the topology is extracted from the end point of the NEB. Therefore, the topologies are more than simple arrangements of vacancies over the lattice nodes because the same set of occupancies can lead to different relaxations.

These topologies are stored, if unknown previously, in the list of known topologies and marked as "unsearched", meaning that if they are visited and occupied during a future energy minimization, they should be searched for new transitions. In addition to topologies, the NEB gives energy barriers that are not exploited by the method, at the moment, but which constitute kinetic information which could be useful either to evaluate at which temperature the transitions could be realistic or opens the possibility for kinetic Monte Carlo with a fixed catalog of rates collected during the MCMC simulation. It can be stressed that the MCMC simulation is richer than the KMC simulations that could be done with the transitions found by the NEB because the Δu moves are sufficient to pass over the low energy barriers and therefore they participate in the exploration of the configuration space.

In the example presented in figures 1 and 2, the acceptance rate is 0.7% for first neighbor exchanges, by SD moves only, between equivalent sites along the tilt axis, in topology 0 (the one with the most extended relaxations). The distribution of the energy variation for SD moves is shifted by almost 3 eV toward low energies in comparison to the distribution for X moves (basic exchange) (Fig. 2c), which confirms that the problem of the overlap of the particles is solved. Nevertheless, there are few attempts that have a negative energy (see insert). One way of improving the acceptance rate is to sample the positions of the particles which are significantly displaced from the lattice nodes during the SD move. For this, the "configurational-bias" Monte Carlo method [34, 42] for growing chain molecules in dense systems has been adapted to the vacancy problem. Originally, a molecule is grown segment by segment by picking the segment's orientation out of k trial orientations. The energy variation related to each trial orientation is calculated and the new orientation is selected according to its Boltzmann weight in the list of trial orientations. It is clear that the probability of selecting this orientation is not random and depends not only on the environment (the configuration of the other molecules in the system), but also on the orientation of the segments previously grown. This probability must be introduced in the acceptance rule and therefore, it must be calculated both for the forward and reverse moves. This means, in the chain molecule example, that the old configuration has to be regrown segment per segment. In the case of vacancy exchange, the same procedure is followed but, instead of choosing orientations for segments, displacements are chosen for neighbors. This is done after the SD move is applied. A list of neighbors with significantly large "darts" is established, typically displacements larger than 0.05 a_0. Nn is the number of such neighbors. The displacements in the "old" configuration are stored as u_i^{old}, to calculate the probability of the reverse move. i refers to the position of the neighbor in the list. Then, sequentially, the "new" displacement for every neighbor u_i^{new} is chosen among Nr random possibilities $u_{ik}^n = r_k\epsilon + u_0^i$. r_k is the k^{th} random vector of the list of length Nr, ϵ is the size of the domain around the component of the dart $\vec{u_0}$ on site i named u_0^i. The energy variation for every of these trial positions is calculated and named $\Delta E(u_{ik}^{new})$. The probability of picking a displacement, for example $u_{ik'}^{new}$, in the list is:

$$p(u_{ik'}^{new}) = \frac{e^{-\Delta E(u_{ik'}^{new})/kT}}{\sum_{k=1}^{Nr} e^{-\Delta E(u_{ik}^{new})/kT}} \tag{3}$$

Once this is done, the index k' is dropped, and after all the neighbors have been treated, the energy of the new configuration is

$$E_{new} = E_{old} + \Delta E_{SD} + \sum_{i=1}^{Nn} \Delta E(u_i^{new}) \tag{4}$$

and the probability of choosing this set of displacements is

$$\prod(o \to n) = \prod_{i=1}^{Nn} p(u_i^{new}) = \frac{e^{-\sum_{i=1}^{Nn} \Delta E(u_i^{new})/kT}}{\prod_{i=1}^{Nn} \sum_{k=1}^{Nr} e^{-\Delta E(u_{ki}^{new})/kT}} \tag{5}$$

For the reverse move: starting from the "new" configuration, the SD move is reverted and then, for each neighbor, $Nr-1$ displacements are selected at random within the ϵ volume around the displacement corresponding to the reversed dart. The corresponding energy variations are calculated and named $\Delta E(u_{ik}^{old})$ and the one for the stored "old" displacement u_i^{old} named $\Delta E(u_i^{old})$. The probability that the old configuration is recovered during the reversed move is:

$$\prod(n \to o) = \frac{e^{-\sum_{i=1}^{Nn} \Delta E(u_i^{old})/kT}}{\prod_{i=1}^{Nn} (e^{-\Delta E(u_i^{old})/kT} + \sum_{k=1}^{Nr-1} e^{-\Delta E(u_{ki}^{old})/kT})} \tag{6}$$

Detailed balance gives the acceptance rule:

$$\begin{aligned} \frac{acc(o \to n)}{acc(n \to o)} &= \frac{\rho_n}{\rho_o} \frac{\prod(n \to o)}{\prod(o \to n)} \\ &= e^{-(\Delta E_{SD} + \sum_{i=1}^{Nn} \Delta E(u_i^{new}))/kT} \frac{\prod(n \to o)}{\prod(o \to n)} \end{aligned} \tag{7}$$

By construction, $\Delta E(u_i^{new})$ tends to be negative, on average. Therefore, in equations 4 and 7, the energy variation related to the SD move, ΔE_{SD}, tends to be decreased by $\sum_{i=1}^{Nn} \Delta E(u_i^{new})$, and therefore, the acceptance rate increased. The term $\frac{\prod(n \to o)}{\prod(o \to n)}$ is complex. Statistics about its distribution have been acquired numerically. It strongly depends on the number Nn of neighbors involved, with a strong tendency to degrade the positive influence of $\sum_{i=1}^{Nn} \Delta E(u_i^{new})$, to an extent where the acceptance rate could be lower than SD moves alone. The strategy followed consist in selecting the neighbors that are the most displaced during the SD move, keeping the number of neighbors low. For example, in the case of

figure 2, a threshold of 0.1 a_0 on the displacements leads to only 4 neighbors involved in the "configurational-bias" procedure. For $N = 1000$, the acceptance rate is 5%, i.e., a boost by a factor of 7 with respect to SD moves alone (SD in Fig. 2c). With a threshold of 0.05 a_0 and 10 neighbors involved, the acceptance rate is only 1.7%. With 4 neighbors, the total computational time of the SD move is only multiplied by a factor of 2 (using 6 threads).

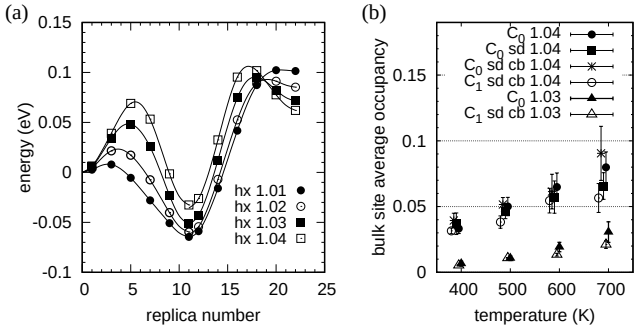

Figure 3. (a) Energy profile between state 1 (replica 0) and state 0 (replica 11) obtained by the NEB, as a function of the homothety factor applied perpendicular to the GB. (b) Occupancy of a bulk site when it is put in equilibrium with the GB either in state 0 or in state 1, as a function of temperature and for two strain levels hx=1.03 and hx=1.04.

Finally, the question of the validation is addressed. The energy variation between states 0 and 1 is shown in figure 3a. The barrier tends to zero when the strain goes to zero, i.e., state 1 (replica 0 in Fig. 3a) is unstable. The barrier is low enough to be crossed by Δu moves only, provided the temperature is high enough. The validation test consists in putting states 0 and 1 in equilibrium with a bulk site by two different paths, using two different MC moves. Path 0 is bulk $\rightleftharpoons$ state 0 $\rightleftharpoons$ state 1, with the first equilibrium established by SD moves and the second by Δu moves. Path 1 is bulk $\rightleftharpoons$ state 1 $\rightleftharpoons$ state 0, with the first equilibrium established by X moves and the second by Δu moves. The X moves have a nonzero acceptance rate because the neighbors are only weakly relaxed toward the vacancy. Figure 3b shows that the two paths lead to the same average occupancies which establishes that the SD moves, including the configurational bias, are properly implemented.

III. APPLICATION TO DIFFERENT GRAIN BOUNDARIES

The method is applied to four symmetrical tilt grain boundaries, two in Al: $\Sigma33(5\bar{5}4)[110]$ [43] (without strain) and $\Sigma13(320)[001]$ [44, 45], and two in bcc Fe: $\Sigma29(730)[001]$ and $\Sigma9(1\bar{1}4)[110]$ [46]. The technical details are given in the appendix. The grain boundary structures, vacancy segregation energies and relaxations when the vacancy occupies the most favorable position are shown in figure 4. The amplitude of the relaxations (u_{max} in table I) is large: between 0.1 and 0.4 a_0 depending on the grain boundary. The efficiency of the Monte Carlo method is evaluated by measuring the acceptance rate for vacancy-particle exchanges in the different structures. To mimic diffusion, exchanges with nearest neighbors were proposed first. When the tilt axis is not aligned with a nearest neighbor pair, the move involves leaving the site that is most favorable energetically and therefore the acceptance is biased by the change in segregation energy. Taking into account this effect, the list of neighbor sites is extended beyond the first neighbors to include the sites that are crystallographically equivalent, along the tilt axis. This means second neighbors for the [100] axis and third neighbors for the [110] axis of the bcc structure. The acceptance rate is measured specifically for moves that do not involve changes in segregation energy. Different degrees of complexity were tested. They are designated in table I as: X for the simple exchange, SD for "Smart Darting" alone and SD+R+b for a Smart Darting exchange combined with a Rosenbluth sampling "R" of neighbor's displacements and inclusion of the corresponding energy bias "b" in the metropolis criterion according to equation 7 (ΔE_{SD} is the energy variation related to SD, $\sum_{i=1}^{Nn} \Delta E(u_i^{new})$ to "R" and $-kT \log \frac{\prod(n\to o)}{\prod(o\to n)}$ to "b"). The reported acceptance rate for the X moves only reflects the absence of acceptance after a large number of trials because of the relaxation of the neighbors shown in Fig. 4. The acceptance rate for SD moves is already very significant: between 1 and 6% depending on the structure. It can be improved up to between 3 and 10% by the SD+R+b move (table I). As already mentioned above, the number of neighbors (Nn) involved in R sampling is crucial and should be minimized. In these tests, they were selected according to the amplitude of their relaxation in the topology with a threshold that is specified by u_{Topo}. Both Nn and u_{Topo} are given in table I. Finally, the "global" acceptance rate is also reported. In this case the moves also involve sites that are not those of optimal segregation energy and therefore less prone to be visited. They are nonetheless important for sampling arrangements of several vacancies.

The process of finding the topologies necessary for the SD moves also produces activation barriers. Although not used in the Monte Carlo simulation, they provide interesting information concerning the kinetics of the vacancies. The effective barrier for diffusion along the tilt axis E_a^{tilt} and the effective barrier to exit the GB E_a^{out} are given in table II. The former is the minimum barrier for a change in the z position of the vacancy and the latter is calculated following the minimum energy path. It is composed of several jumps and stops when the vacancy bulk activation barrier is recovered. The local minima along the path form a basin where, as a first approximation, the occupancies are considered equilibrated before the exit event [47]. The escape rate (through the path) is the product of the probability of being in the last local minimum along the path times the frequency for crossing the last barrier. If the bottom of the basin has a signifi-

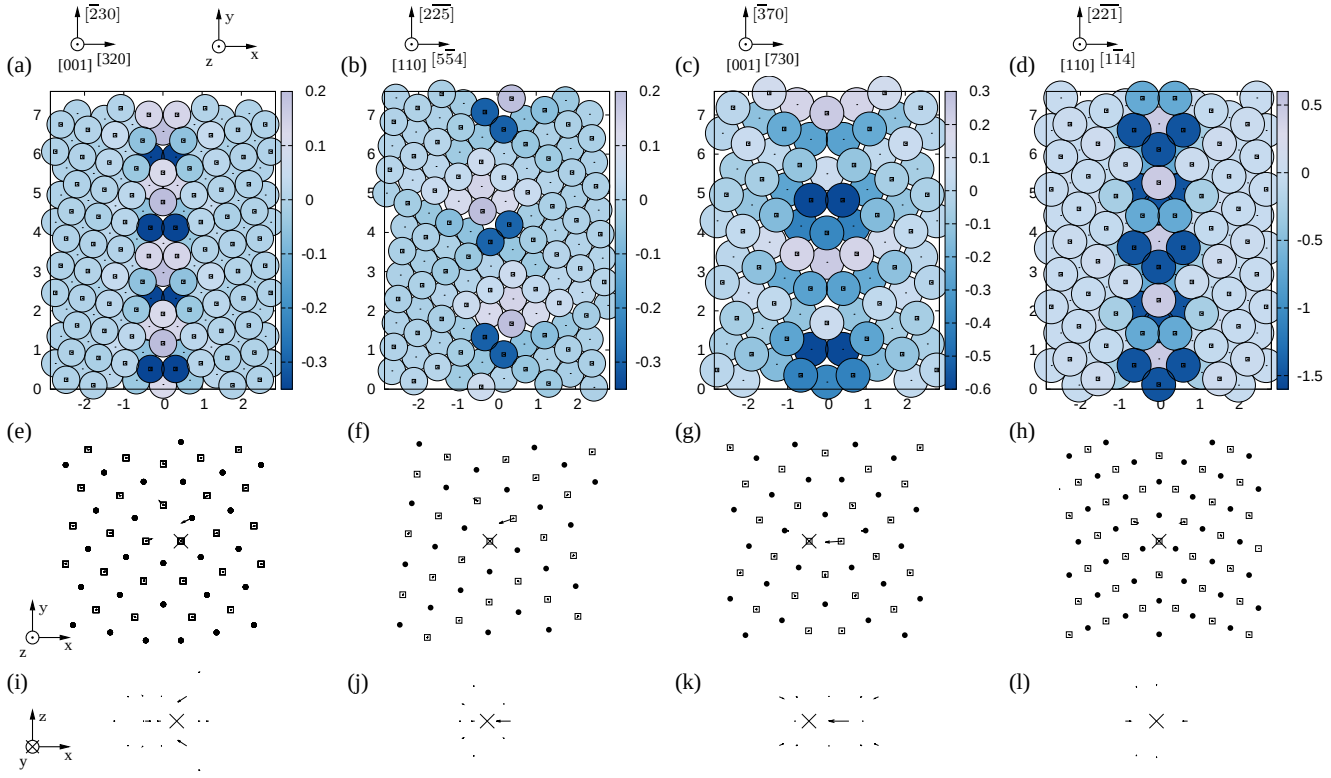

Figure 4. (Color online) Symmetrical tilt grain boundary structures without vacancies: (a) Σ13(320)[001], (b) Σ33(5$\bar{5}$4)[110] in Al and (c) Σ29(730)[001], (d) Σ9(1$\bar{1}$4)[110] in bcc Fe. Colors represent the vacancy segregation energy (ΔE_{seg}). The minimum values are given in table II. The relaxations around a single vacancy in this optimal configuration are represented by arrows on (e,f,g,h) projected in the (x,y) plane and in the (x,z) plane on (i,j,k,l) (only the displacements are shown). The vacant site is marked by a large cross.

cantly lower energy than the others, the prefactor ahead of the final rate can be approximated. Then, the effective energy barrier for exiting the basin is simply the difference in segregation energy between the bottom of the basin and the last state before exit added to the last jump barrier. It is this value which is reported as the effective barrier for exiting the GB. The vacancy diffusion along the grain boundaries is found to be significantly dependent on the structure (as already known from MD simulations of self-diffusion [48]). The exit barrier is always much larger than the bulk barrier. It is close to, but not exactly equal to, the difference between the bulk activation energy and the segregation energy. In contrast, the activation energy for diffusion along the tilt axis can be larger, or smaller than the bulk value, meaning that intergranular vacancies do not necessarily diffuse faster than bulk vacancies. Nevertheless, self-diffusion is faster than in the bulk because the vacancy formation energy is decreased. Finally, for these grain boundaries, the diffusion occurs along the tilt axis with no easy path to move from one structural unit to the other (i.e. in the y direction). The activation energy in the y direction can be taken, as an approximation, as the exit activation energy.

The aggregation of two vacancies is also studied by the MCMC method. Each grain boundary studied exhibits a different behavior. The results of the simulations dedicated to the two GBs in Al are reported in Figure 5, those in Fe are discussed in the Supplemental Material. The inserts (Fig. 5 a and b) represent the position of the vacancies along the tilt axis of the GBs along the Markov chain. Periodic boundary conditions are applied. The length of the simulation box is 12 periods in both cases but one period is 1 a_0 long for the Σ13 of axis [001] and $\sqrt{(2)}/2$ a_0 for the Σ33 of axis [110]. Therefore, the nearest crystallographically equivalent sites along the tilt axis are a second neighbor and a first neighbor, respectively. Both inserts demonstrate that the z positions are well sampled. The clustering tendency is very different. In the Σ13 case, the distance between the vacancies (d) fluctuates between 1 and $L_z/2$, which is the maximum separation allowed by the periodic boundary conditions. The energy of the topologies "visited"is superimposed to d. This energy is the one found after minimization when the topology is extracted. It is not the current energy of the system. "Visited" is to be taken in the "Smart Darting" sense, i.e., the distance between the microstate and the local energy minimum is lower than the threshold defining the neighborhood of the local minimum in

Table I. Acceptance rates for exchange moves between equivalent sites along the tilt axis, with different types of moves: X simple exchange, SD Smart Darting move, SD+R+b Smart Darting move combined with a Rosenbluth sampling of the Nn neighbors of the vacancy that have a displacement larger than u_{Topo}. u_{max} is the maximum amplitude the relaxations. The "global" acceptance rate is also given. Numbers in parentheses are the mean square difference obtained from 4 independent runs.

	Σ13	Σ33	Σ29	Σ9
SD	0.011 (0.003)	0.018 (0.001)	0.016 (0.001)	0.066 (0.004)
SD+R+b	0.046 (0.001)	0.058 (0.003)	0.030 (0.001)	0.102 (0.003)
global	0.010 (0.0002)	0.011 (0.0002)	0.005 (0.0002)	0.014 (0.0003)
X	$< 6\,10^{-5}$	$< 4\,10^{-5}$	$< 4\,10^{-5}$	$< 10^{-4}$
Nn	2	1	1	2
u_{max} (a_0)	0.23	0.30	0.40	0.11
u_{Topo} (a_0)	0.2	0.1	0.2	0.1

Table II. Bulk vacancy formation energy, vacancy segregation energy on the most favorable site, energy barrier for an exchange between a vacancy and a first neighbor in a perfect cristal environment, effective energy barrier for diffusion along the tilt axis of the GB.

	Σ13	Σ33	Σ29	Σ9
E_f^{bulk}	0.68	0.68	2.10	2.10
ΔE_{seg}	-0.43	-0.29	-0.64	-1.49
E_a^{bulk}	0.65	0.65	0.68	0.68
E_a^{tilt}	0.82	0.61	0.76	0.97
E_a^{out}	0.99	0.94	1.13	2.15

SD. The energy variations are small, lower than 0.05 eV. The minimum energy found is a configuration where the vacancies are separated by a distance of 2 a_0. The saddle searches have explored configurations with d<1 and their energies are higher than the minimum by 0.4 to 0.6 eV, which might explain why transitions from micro states with d=1 to those with d<1 are not observed. In contrast, in the Σ33 case, the vacancies bind. The evolution of d (Fig. 5b) illustrates how the algorithm explores new configurations that enrich the list of topologies, which opens new transitions for Smart Darting, such as transitions with smaller and smaller d. The simulation is started with d maximum and the list of topologies obtained for the single vacancy. First, d fluctuates with values larger than 3 times the period in z until the method learns the configurations where d is equal to 2 periods. Then, these configurations are visited without significant energy changes, and from there, the method finds the configuration where the vacancies bind in first neighbor position. The energy drops by approximately 0.3 eV. Beyond this point, the energy fluctuates with an amplitude as high as 0.5 eV, and the cluster moves along the tilt axis, without complete splitting (insert Fig. 5b). In the case of Fe, the vacancies bind by more than 1 eV in the Σ29 and form pairs along the tilt axis with a separation of one period (1 a_0). In the Σ9 case, they repel each other by 60 meV and therefore remain split (see the Supplemental Material).

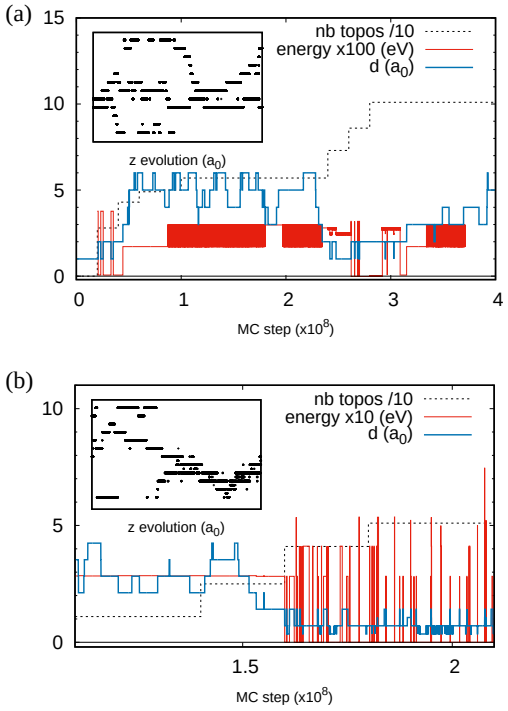

Figure 5. (Color online) Evolution of the distance between the vacancies, the energy of the topology visited and the number of topologies detected along the Markov chain for a system containing two vacancies: (a) Σ13(320)[001], (b) Σ33(5$\bar{5}$4)[110] in Al. The position in z (the tilt axis direction) is shown on the insert.

IV. DISCUSSION AND CONCLUSION

One interesting question about intergranular vacancies is whether their specific structure, qualified as "delocalized", leads to specific properties or if they behave in a

similar way as in the bulk. Regarding diffusion, our findings are similar to what is summarized in the introduction: several sites lead to the delocalized structure (the dark sites in Fig. 4) which means that long jumps can be expected when entering the GBs. In contrast, once the vacancy is in the optimum location, saddle searches have not revealed any low energy path for diffusing out of this configuration and the barriers are similar to bulk diffusion (Tab. II). The elastic field produced is analyzed by calculating the elastic dipole tensor P_{ij} (Tab. IV), via the Kanzaki forces [49]. Convergence of the calculation with the number of neighbor shells gives an estimate of the range of the elastic deformation produced by the defect. The influence of the number of shells restored [49, 50] gives an estimate of the range of the anharmonic region around the defect. The range of the elastic field is approximately 3 a_0, similar to the bulk (r_e in table IV). In contrast, the range of the anharmonic relaxations can be much larger in the GBs, up to 1.75 a_0. These values are coherent with the radius used for defining the topologies (2.5 a_0) which was found empirically by increasing the radius until no configuration built from the topologies relaxed toward a different minimum than the one targeted. Furthermore, the amplitude of P_{ij} in the GBs can be approximately twice that in the bulk (Tab. IV). This suggests that an external elastic field could have a significant impact on the segregation energies. Indeed, the magnitude of this difference, typically 4 eV, leads to interaction energies of the same order of magnitude as the segregation energies for reasonably large elastic strains. For example, 2% normal strain ϵ_{11} leads to $\Delta E_e = -(P_{ij}^{gb} - P_{ij}^{bulk})\epsilon_{ij}^{ext} \sim 0.08$ eV which is already of the order of 20% of the segregation energy (Tab.4). In contrast, the calculation of the vacancy-vacancy elastic interaction energy, from the P_{ij} and within isotropic elasticity (the Al case), gives a negligible interaction (on the order of 1 meV in first neighbor along the tilt axis of $\Sigma 33$). The binding energies found, which are therefore pure core effects, depend on the structure and are different from the bulk values: -0.02 eV, 0.3 eV, 1 eV and -0.06 eV for $\Sigma 13$, $\Sigma 33$, $\Sigma 29$ and $\Sigma 9$, respectively, while in the bulk the interaction is zero in Al [51] and 0.14 and 0.3 eV in the first and second nearest neighbor positions in Fe [52]. Additionally, because the segregation energies are large, the interactions are along the tilt axis in every case. In brief, the differencies between a bulk and a delocalized intergranular vacancy are a strong anisotropy for diffusion, which is essentially along the tilt axis, an enhanced elastic interaction with external elastic fields and a structure-dependent tendency of forming one-dimensional chains, in the 4 structures studied, which are pure tilt. Note that the binding is quite different in twist grain boundaries where vacancies accumulate at the intersections of screw dislocations [53].

In conclusion, the paper presents an extension of Markov chain Monte Carlo that overcomes the limitations of the vanishing acceptance rate for particle exchanges in the case of large relaxations. The method is illustrated in the particularly demanding case of delocalized intergranular vacancies. The Monte Carlo moves are composed of the classical random particle displacements and vacancy-particle exchanges, to which "Smart Darting" moves are added. They are based on a list of topologies built on the fly, which contain the relaxations around the vacancies in the configurations of local minimum potential energy. When the system enters a neighborhood of one such minimum, it can be transported in the vicinity of another minimum of the list. In the vacancy case, the move consists in erasing the relaxations of the neighbors of the vacancy before inserting a particle at its location and creating the appropriate relaxations at its new location. Taking four different tilt boundaries, it is shown that the occupancy of the crystallographically equivalent sites along the tilt axis can be sampled with acceptance rates of several % at room temperature. These high rates are obtained when, in addition to "Smart Darting", the positions of key neighbors are also sampled. Note that if the relaxations are dilatations, a similar but simpler algorithm exists [54]. Divacancies were also studied by the method. They exhibit GB-specific behaviors such as: permanent binding, dissociation followed by immediate binding or no interaction at all. Additional data are reported that could be useful to build mesoscale models: elastic dipole tensors, activation barriers for 1D diffusion along the tilt axis and effective barriers to exit the GB or diffuse perpendicular to the tilt axis. Future work will consist in sampling intergranular vacancy configurations beyond 2 vacancies and under the influence of an external strain, since the use of particle displacements enables equilibrating stresses when applying a displacement on the side of the system. The effect of elastic strains on intergranular vacancies seems particularly strong and is important in the context of ductile fracture [1], including under irradiation [55], and in thin films [56] when discussing the existence of cavities.

ACKNOWLEDGMENTS

This project has received funding from the Euratom research and training programme 2014-2018 under grant agreement No 755039. A. F. Voter and D. Perez (Los Alamos National Laboratory) kindly introduced me to the Smart Darting method and k-ART during numerous visits at LANL funded by the CNRS-pics program and LANL.

Appendix A: Technical details

The particles interact by EAM potentials: reference [57] for Al and [52] for Fe. The box sizes are given in table III and the crystallographic directions in figure 4. Periodic boundary conditions are applied in the y and z directions and two regions are fixed on the sides perpendicular to the x direction (the normal to the GBs). The

width of the rigid regions is the range of the potential plus $0.5a_0$. The main parameters for SD are: $\epsilon = 0.2$ a_0, the size of the neighborhood around the local energy minima, the radius around the vacancy for defining the topology is 2.5 a_0 in the plane perpendicular to the tilt axis and 2.2 a_0 along the tilt axis and the number of random displacements per atom in the Rosenbluth sampling $Nr = 1000$. Note that the displacements are taken within a cube of side ϵ, therefore it is a dense sampling.

Table III. Simulation box sizes L_x, L_y, L_z (a_0), number of atoms nat, and coincidence site lattice cell size CSL_x, CSL_y, CSL_z (a_0).

	Σ13	Σ33	Σ29	Σ9
L_x (a_0)	31.3	32.2	15.6	33.8
L_y (a_0)	14.4	11.5	15.2	12.0
L_z (a_0)	12.0	8.48	16	17.0
nat	19776	12528	7232	13632
CSL_x (a_0)	7.2	8.12	7.6	8.48
CSL_y (a_0)	7.2	5.74	7.6	6.0
CSL_z (a_0)	1.0	0.71	1.0	1.41

Appendix B: Elastic dipole tensor

Table IV. Components of the elastic dipole tensor P_{ij} (eV) for a vacancy in bulk Al and Fe and in the four grain boundaries, in the favorable configuration (Fig. 4), computed from the Kanzaki forces [49]. The range of the elastic distortions r_e and of the anharmonicity r_a are also given (a_0).

	bulk Al	Σ13	Σ33	bulk Fe	Σ29	Σ9
P_{11} (eV)	-3.9	-11.2	-7.5	-1.3	-21.0	-7.8
P_{22} (eV)	-3.9	-8.8	-3.3	-1.3	-4.0	-8.2
P_{33} (eV)	-3.9	-4.5	-7.2	-1.3	-11.8	-7.1
P_{12} (eV)	0.0	-4.0	-2.3	0.0	-0.3	0.0
P_{13} (eV)	0.0	0.0	0.0	0.0	0.0	0.0
P_{23} (eV)	0.0	0.0	0.0	0.0	0.0	0.0
P_{11} (eV)	-2.5[a]			-3.6[b]		
r_e (a_0)	2.5-3.	3.	3.	3.5	3.5	3.5
r_a (a_0)	0.7	1.58	1.75	1.41	1.75	1.75

[a] DFT value from reference [58]
[b] DFT value from reference [59]

[1] P. J. Noell, R. Sills, A. A. Benzerga, and B. L. Boyce, Void nucleation during ductile rupture of metals: a review, Prog. Mat. Sci. **135**, 101085 (2023).
[2] P. J. Noell, J. E. Sabisch, D. L. Medlin, and B. L. Boyce, Nanoscale conditions for ductile void nucleation in copper: Vacancy condensation and the growth-limited microstructural state, acta mater **184**, 211 (2020).
[3] P. Lukáš, L. Kunz, L. Navrátilová, and O. Bokůvka, Fatigue damage of ultrafine-grain copper in very-high cycle fatigue region, Mat. Sci. Eng. A **528**, 7036 (2011).
[4] T. Miura, K. Fujii, and K. Fukuya, Micro-mechanical investigation for effects of helium on grain boundary fracture of autenitic stainless steel, Journal of nuclear materials **457**, 279 (2015).
[5] D. Tanguy, Cohesive stress heterogeneities and the transition from intrinsic ductility to brittleness, Phys. Rev. B **96**, 174115 (2017).
[6] G. M. Scamans, R. Alani, and P. R. Swann, Pre-exposure embrittlement and stress corrosion failure in AlZnMg alloys, Corros. Sci. **16**, 443 (1976).
[7] M. L. Martin, B. P. Somerday, R. O. Ritchie, P. Sofronis, and I. M. Robertson, Hydrogen-induced intergranular failure in nickel revisited, Acta Materialia **60**, 2739 (2012).
[8] I. M. Robertson, P. Sofronis, A. Nagao, M. Martin, S. Wang, D. Gross, and K. Nygren, Hydrogen embrittlement understood, Metallurgical and materials transaction A **46A**, 2323 (2015).
[9] M. L. Martin, I. M. Robertson, and P. Sofronis, Interpreting hydrogen-induced fracture surfaces in terms of deformation processes: A new approach, acta mater. **59**, 3680 (2011).
[10] J. Huang, M. Meyer, and V. Pontikis, Is pipe diffusion in metals vacancy controlled' a Molecular-Dynamics of an edge dislocation in copper, Phys. Rev. Lett. **63**, 628 (1989).
[11] J. von Boehm and R. M. Nieminen, Molecular-dynamics study of partial edge dislocations in copper and gold: Interactions, structures, and self-diffusion, Phys. Rev. B **53**, 8956 (1996).
[12] Q. F. Fang and R. Wang, Atomistic simulation of the atomic structure and diffusion within the core region of an edge dislocation in aluminum, Phys. Rev. B **62**, 9317 (2000).
[13] A. Suzuki and Y. Mishin, Atomic mechanisms of grain boundary diffusion: Low versus high temperatures, Journal Of Materials Science **40**, 3155 (2005).
[14] A. Suzuki and Y. Mishin, Interaction of point defects with grain boundaries in fcc metals, Interface Science **11**, 425 (2003).
[15] A. Suzuki and Y. Mishin, Atomistic modeling of point defects and diffusion in copper grain boundaries, Interface Science **11**, 131 (2003).
[16] M. Sørensen, Y. Mishin, and A. Voter, Diffusion mechanisms in cu grain boundaries, Physical Review B **62**, 3658 (2000).
[17] H. Zhang, D. J. Srolovitz, J. F. Douglas, and J. A. Warren, Atomic motion during the migration of general [001] tilt grain boundaries in ni, acta mater. **55**, 4527 (2007).
[18] H. Zhang, D. J. Srolovitz, J. F. Douglas, and J. A. Warren, Characterization of atomic motion governing grain boundary migration, Phys. Rev. B **74**, 115404 (2006).
[19] T. Frolov, D. L. Olmsted, M. Asta, and Y. Mishin, Structural phase transformations in metallic grain boundaries, Nature Comm. **4**, 1899 (2013).

[20] A. P. Sutton and R. W. Balluffi, *Interfaces in Crystalline Materials* (Oxford Science Publications, 1995).

[21] J. Han, V. Vitek, and D. J. Srolovitz, The grain-boundary structural unit model redux, acta mater. **133**, 186 (2017).

[22] J. Han, V. Vitek, and D. J. Srolovitz, Grain-boundary metastability and its statistical properties, acta mater. **104**, 259 (2016).

[23] W. Han, M. Demkowicz, E. Fu, Y. Wang, and A. Misra, Effect of grain boundary character on sink efficiency, acta mater. **60**, 6341 (2012).

[24] J. Han, V. Vitek, and D. J. Srolovitz, The interplay between grain boundary structure and defect sink/annealing behavior, IOP Conf. Series: Materials Science and Engineering **89**, 012004 (2015).

[25] K. Kolluri and M. J. Demkowicz, Formation, migration, and clustering of delocalized vacancies and interstitials at a solid-state semicoherent interface, Phys. Rev. B **85**, 205416 (2012).

[26] W. S. Yu and M. J. Demkowicz, Non-coherent cu grain boundaries driven by continuous vacancy loading, J. Mater. Sci. **50**, 4047 (2015).

[27] W. Jäger and H. Trinhaus, Defect ordering in metals under irradiation, J. Nucl. Mat. **205**, 394 (1993).

[28] Y. Gao, Y. Zhang, D. Schwen, C. Jiang, C. Sun, J. Gan, and X.-M. Bai, Theoretical prediction and atomic kinetic Monte Carlo simulations of void superlattice self-organization under irradiation, sci. rep. **8**, 6629 (2018).

[29] R. J. Zamora, B. P. Uberuaga, D. Perez, and A. F. Voter, The modern temperature-accelerated dynamics approach., Annu. Rev. Chem. Biomol. Eng. **7**, 87 (2016).

[30] D. Perez, E. D. Cubuk, A. Waterland, E. Kaxiras, and A. F. Voter, Long-time dynamics through parallel trajectory splicing., J. Chem. Theory Comput. **12**, 18 (2016).

[31] G. Henkelman and H. Jónsson, Long time scale kinetic monte carlo simulations without lattice approximation and predefined event table., J. Chem. Phys. **115**, 9657 (2001).

[32] L. K. Béland, P. Brommer, F. El-Mellouhi, J.-F. Joly, and N. Mousseau, Kinetic activation-relaxation technique, Phys. Rev. E **84**, 046704 (2011).

[33] R. B. Garza, J. Lee, M. H. Nguyen, A. Garmon, D. Perez, M. Li, J. C. Yang, G. Henkelman, and W. A. Saidi, Atomistic mechanisms of binary alloy surface segregation from nanoseconds to seconds using accelerated dynamics, J. Chem. Theory Comput. **18**, 4447 (2022).

[34] D. Frenkel and B. Smit, *Understanding Molecular Simulation* (Academic Press, 2002).

[35] A. Seki, D. N. Seidman, Y. Oh, and S. M. Foiles, Monte carlo simulations of segregation at [001] twist boundaries in a pt(au) alloy-i. results, Acta metall. mater. **39**, 3167 (1991).

[36] R. K. Koju and Y. Mishin, Relationship between grain boundary segregation and grain boundary diffusion in Cu-Ag alloys, Phys. Rev. Materials **4**, 073403 (2020).

[37] I. Andricioaei, J. E. Straub, and A. F. Voter, Smart darting monte carlo, J. Chem. Phys. **114**, 6994 (2001).

[38] S. M. Foiles, Calculation of the surface segregation of Ni-Cu alloys with the use of the embedded-atom method, Phys. Rev. B **32**, 7685 (1985).

[39] D. Tanguy and M. Mareschal, Superabundant vacancies in a metal-hydrogen system: Monte carlo simulations, Phys. Rev. B **72**, 174116 (2005).

[40] E. Vamvakopoulos and D. Tanguy, Equilibrium vacancy concentrations in al-$\sigma = 33(554)[110]$ by grand canonical monte carlo simulations, Phys. Rev. B **79**, 094116 (2009).

[41] H. Jónsson, G. Mills, and K. Jacobsen, *Classical and Quantum Dynamics in Condensed Phase Simulations* (World Scientific, Singapore, 1998) p. 385.

[42] D. Frenkel, G. C. A. M. Mooij, and B. Smit, Novel scheme to study structural and thermal properties of continuously deformable molecules, J. Phys. Condens. Matter **4**, 3053 (1992).

[43] J. Rittner and D. Seidman, [110] symmetric tilt grain-boundary structures in fcc metals with low stacking-fault energies, Physical Review B **54**, 6999 (1996).

[44] Y. Mishin, A. Suzuki, B. Uberuaga, and A. Voter, Stick-slip behavior of grain boundaries studied by accelerated molecular dynamics, Physical Review B **75**, 224101 (2007).

[45] A. Rajabzadeh, F. Mompiou, M. Legros, and N. Combe, Elementary mechanisms of shear-coupled grain boundary migration, Phys. Rev. Lett. **110**, 265507 (2013).

[46] M. A. Tschopp, K. N. Solanki, F. Gao, X. Sun, M. A. Khaleel, and M. F. Horstemeyer, Probing grain boundary sink strength at the nanoscale: Energetics and length scales of vacancy and interstitial absorption by grain boundaries in α-fe, Phys. Rev. B **85**, 064108 (2012).

[47] B. Puchala, M. L. Falk, and K. Garikipati, The Journal of Chemical Physics **132**, 134104 (2010).

[48] Y. Mishin, M. Asta, and J. Li, Atomistic modeling of interfaces and their impact on microstructure and properties, acta mater. **58**, 1117 (2010).

[49] E. Clouet, C. Varvenne, and T. Jourdan, Elastic modeling of point-defects and their interaction, Comp. Mat. Sci. **147**, 49 (2018).

[50] G. Simonelli, R. Pasianot, and E. J. Savino, Point-defect computer simulation including angular forces in bcc iron, Phys. Rev. B **50**, 727 (1994).

[51] H. Wang, D. Rodney, D. Xu, R. Yang, and P. Veyssière, Pentavacancy as the key nucleus for vacancy clustering in aluminum, Phys. Rev. B **84**, 220103(R) (2011).

[52] L. Malerba, M. Marinica, N. Anento, C. Björkas, H. Nguyen, C. Domain, F. Djurabekova, P. Olsson, K. Nordlund, A. Serra, D. Terentyev, F. Willaime, and C. Becquart, Comparison of empirical interatomic potentials for iron applied to radiation damage studies, Journal of Nuclear Materials **406**, 19 (2010).

[53] E. Martínez and A. Caro, Atomistic modeling of long-term evolution of twist boundaries under vacancy supersaturation, Phys. Rev. B **86**, 214109 (2012).

[54] H. B. Lee, F. B. Prinz, and W. Cai, Atomistic simulations of surface segregation of defects in solid oxide electrolytes, Acta Mater. **58**, 2197 (2010).

[55] L. M. et al., Multiscale modelling for fusion and fission materials: The m4f project, Nuclear Materials and Energy **29**, 101051 (2021).

[56] S. Curiotto, A. Chame, P. Müller, C. V. Thompson, and O. Pierre-Louis, Hole opening from growing interfacial voids: A possible mechanism of solid state dewetting, Appl. Phys. Lett. **120**, 091603 (2022).

[57] Y. Mishin, D. Farkas, M. J. Mehl, and D. A. Papaconstantopoulos, Interatomic potentials for monoatomic metals from experimental data and ab initio calculations, Phys. Rev. B **59**, 3393 (1999).

[58] D. D. Fonseca, F. Onimus, F. Mompiou, M.-C. Marinica, E. de Sonis, E. Clouet, and T. Jourdan, Numerical investigation of dislocation climb under stress and irradiation, acta mater. **242**, 118431 (2023).

[59] J. S. Wróbel, M. R. Zemła, D. Nguyen-Manh, P. Olsson, L. Messina, C. Domain, T. Wejrzanowski, and S. L. Dudarev, Elastic dipole tensors and relaxation volumes of point defects in concentrated random magnetic fe-cr alloys, comp. mat. sci. **194**, 110435 (2021).